IRC-SET 2015

Level: **Junior College**

Project Title: **Cloud Detection and Monitoring**

Team Member: **Loh Yi Chang**
Mentor: **Assoc. Prof. Lee Yee Hui**
Mr Chua Chee Siang
Mr Lee Kang Hao
School: **Yishun Junior College**

Contents

1. Introduction

Radio Frequency Interference (RFI) is a form of distortion of radio waves which could result in loss of data transferred in between the source and receiver (Hallas, 2009). This is a significant problem in modern warfare as information being relayed through radio telecommunication is very prominent (Kenyon, 2012).

Radio telecommunication works by transmitting radio waves from a source to a receiver that translates the radio waves into information. Range of radio waves are enhanced by using a satellite (Ford, 2000). Radio waves would pass through Earth's atmosphere, one of which being the ionosphere. A layer which contains high density of free electrons owing to solar radiation. The ionosphere could thus reflect and absorb radio waves, leading to RFI (Radio Jove Nasa, 2006). Due to the nature of the ionosphere and depending on the time of day, lower frequencies would not be able to pass through the ionosphere while higher frequencies would be weakened (Poole, 1999; Camalan, 2006). Like the ionosphere, clouds interfere with radio waves in a similar manner. Clouds affect radio waves with charged particles absorbs the radio waves and cause RFI (Phatz, Herrmann, & Shinbrot, 2010). The research between MINDef and NTU aims to examine the relationship between clouds and RFI. Integral to the research, this project will focus on the equipment optimisation aspect of capturing cloud images to be used for the research analysis.

2. Investigative Approach

The aim of this investigation was to find suitable free HDRI software that fits the needs of this project. Different Exposure Values (EV) were experimented with to produce an optimal HDRI of the sky and clouds. The quality of the resulting images from the HDRI software and the different EV were determined objectively by a MATLab assessment code (ANNEX B). The result would be an optimised configuration that could be used in the accurate and precise 3-dimensional reconstruction of the sky.

3. Methodology

6.1 High Dynamic Range Image Processing

HDRI Processing is a technique used by photographers to produce high fidelity photos. It uses a set of photographs of the same scene but with different dynamic range. Once the photographs were imported into a HDRI software, it would merge the set of photographs into a HDRI. HDRI have a greater dynamic range when compared to normal photographs, thus revealing more information that sometimes may be masked in normal photographs due to the lack of dynamic range. As visible in Figure 1, more leaves could be seen at the top of the HDRI as compared to the Orignial image.

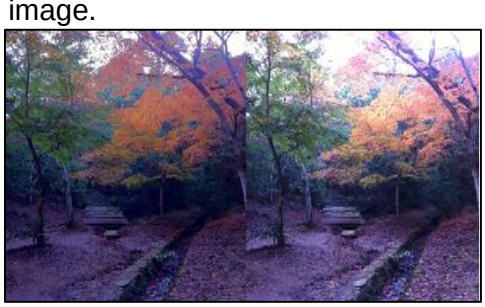

HDRI Original

Figure 1. Comparison between HDRI and Original image

Using HDRI will be suitable as the research involves taking sky images where the sun was present. HDRI would be able to compensate the glare and high contrast from the sun so that the clouds become more visible and detailed. (Stumpfel, et al., 2004) For this research, three HDRI software would be compared, Fusion_F1, Luminance, Picturenaut.

6.2 MATLab Code Quality assessment

Visual inspection of HDRI was subjective in determining the quality of the HDRI. To assess it objectively, a MATLab code would identify four aspects of the HDRI as follows:

1. Percentage of clipped pixels was determined to quantify the pixel distortion. It was best to have minimum clipped pixels since the HDRI require as much details as possible.
2. Percentage of 'unused' parts of the dynamic range was measured in the code. This determines how much information was unused from the different dynamic ranges to form the HDRI. This should be as low as possible.
3. Measurement of the centre of pixels distribution determines how much the image deviates from the centre of the dynamic range. HDRI merge three images of different EV. E.g: Exposure bracket (+2, 0,-2), EV(0) will be used as the centre of the dynamic range. The code will identify how much the HDRI has deviated from the original EV(0).
4. Amount of gradient in the image finds out how much contrast there is in the image. This helps to differentiate the sky from the clouds as well as aiding in the precision of the results.

Using this code would help to better assess the images objectively and determine which HDRI software and EV was the best (ANNEX B).

6.3 Sky Imager

A total of three sets of sky images were captured using an automated sky imager that could be controlled remotely from a computer. Table 1 shows the final settings for the sky imager as a result of this project.

Table 1: Final Camera Settings

Camera settings:	
Model	Canon EOS 600D
ISO speed	ISO-100
Aperture Value (F-stop)	f/22
Mode	Aperture Priority
Flash	No flash
Focal length	5mm
Lens	Fish-eye lens

4. Findings

7.1 Set 1: Testing for Optimal Aperture Values

Set 1 was used to determine whether the AV would be a factor in the quality of HDRI processed. It consists of four groups with only differing Aperture Values (AV) and the same EV of (+2, 0,-2). AV of 4, 8, 16 and 22 was captured with the same portion of sky.

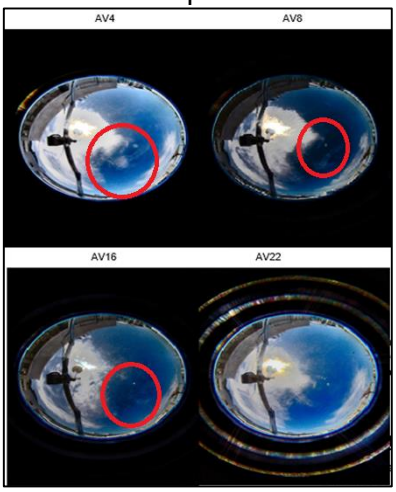

Figure 2. Set 1 results

AV22 produced the best results out of the four groups. The other three groups had clipped pixels around the edge of the clouds, which were circled in their respective HDRIs, whereas there are none for AV22 in Figure 2. These clipped pixels were also known as pixels with distorted colour that reduces the quality of the HDRI. Thus, AV was a factor to the quality of HDRI and further sets would have the AV locked to 22. The sun blocker could be seen across the lens (Fig 2). However, the sun blocker was not effective in blocking out the sun and could

be observed to be producing unwanted glares around it (Fig. 2). Hence, for the rest of the experiments, the sun blocker would not be used.

7.2 Set 2: Testing for Optimal Exposure Values (EV)

Set 2 consists of 11 groups with differing EV, ranging from +4 to -4. The AV was set at 22 for all 11 groups. In addition, Set 2 was also used to test how HDRI fares in taking images of the open sky without the sun blocker (Stumpfel, et al., 2004). Set 2 would aim to find out the best software and bracketed EVs to use. EV higher and lower than +4 and -4, respectively, would not be used as it takes a long duration to capture them. If the time taken to capture the photos was too long, the clouds may have moved and the three exposures used for HDRI would not have the same identical image. As there are 11 groups, only significant photos which presented flaws or strengths would be presented.

Figure 3. Colour Distortion

Some results of set 2 had shown anomalies as shown in Figure 3. These HDRI shown had their colours distorted or oversaturated (Fig. 3). This was to be avoided as we lose the data of its original colour for 3-dimensional reconstruction.

Set 2 was processed through the 3 HDRI software, producing a total of 33 HDRI which were all run through the Quality Assessment in MATLab (ANNEX A). Fusion_F1 came out on top as it produced the most consistent results whereas the other 2 software had abrupt rise and fall in quality throughout the 11 groups. EV (+2, 0, -2) was the best as it had the best of the four aspects out of the others.

7.3 Set 2.5: Experimenting with a different Post Process

Set 2 was also used to experiment with another image post process, SUMMATION (SUM) that also produces similar results to HDRI processing. SUM picked out the best parts of photos of different EV to form a higher detailed photo instead of merging all the photos together like HDRI processing. The images were processed through Fusion_F1 which have both HDRI and SUM processing capabilities.

HDRI SUM

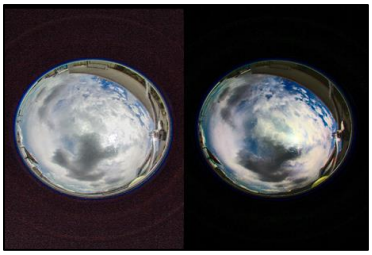

Figure 4. HDRI and SUM comparison

SUM had produced images that had colour distortion. The colours from these images do not reflect the true colours of the original image as closely as that of HDRI. Therefore, HDRI will still be used.

7.4 Set 3: Experiment for Direct Capture of the Sun

Set 3 consisted of 19 groups with EVs ranging from +2 to -2. The aim of Set 3 was to find out how well would HDRI fare with the direct capture of the sun. In the previous sets, images were taken beneath a plastic dome that protects the camera lens from dust. However, the plastic dome introduced unnecessary artefacts into the image as well as unwanted glares.

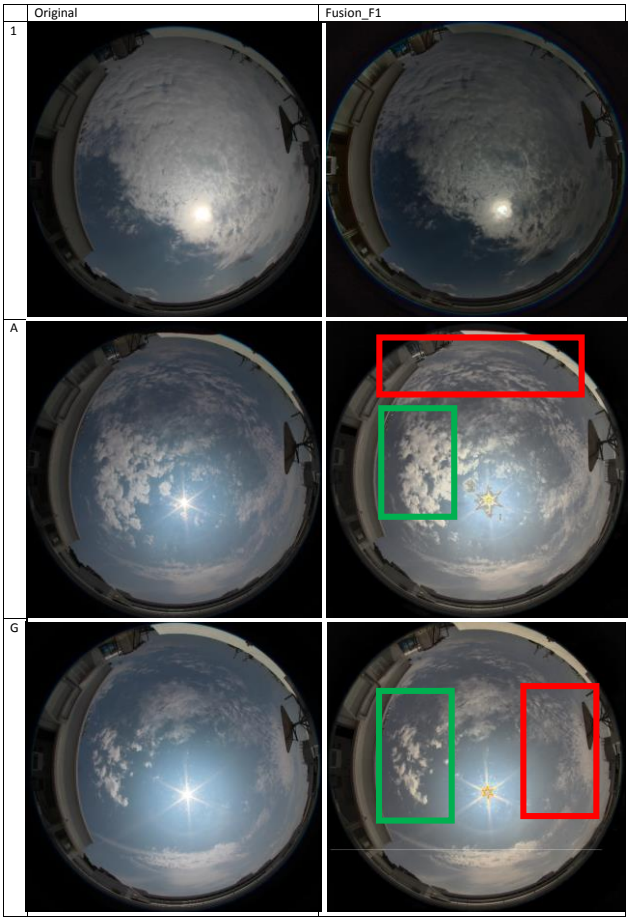

Figure 5. Original and HDRI comparison

The result was apparent with greater details from the HDRI as compared to the originals along with the direct capture of the sun producing far more details of the clouds than the original. Subset A and G (Fig. 5) show that not only are there more details, the HDRI yield better depth of field too. Clouds closer to the ground were shown to be brighter and the ones further away were shown to be darker with the clouds further away in red boxes and closer in green boxes.

7.5 Analysis of findings by comparing the three software

The following results are taken from the 11 groups of images in Set 2. All 11 groups produced 11 HDRI each with each HDRI software. All 33 HDRI were then assessed objectively through the MATLab code (ANNEX B) and compared below. The Highest value, Average value and Lowest value of the 11 groups would be taken. They will be used to compare the performance of the three software.

7.5.1 Clipped Pixels

The three software generally have similar Highest percentage value and Average percentage value (Fig. 6). However, Fusion_F1 has the Lowest percentage value, followed by Picturenaut and then Luminance. This shows that Fusion_F1 has the potential to produce the least amount of clipped pixels out of the three software.

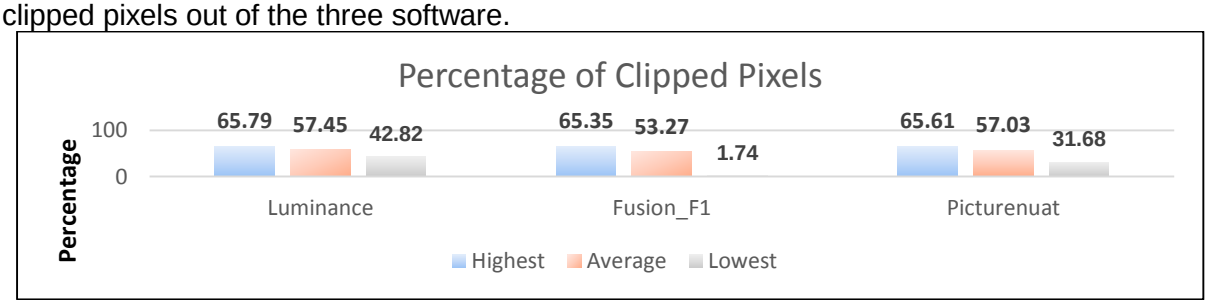

Figure 6. Graph of Percentage of clipped pixels

7.5.2 Unused Data from Dynamic Range

Luminance has the lowest percentage value, followed by Picturenaut and lastly, Fusion_F1.

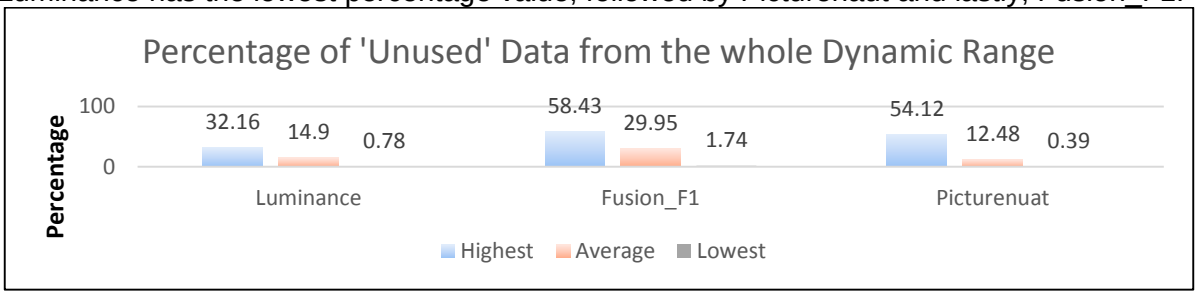

Figure 7. Graph of Percentage of 'Unused' Data from the whole dynamic range

7.5.3 Deviation of pixels from the Centre of Distribution

The proportion of the total number of pixels the results are similar for all three software, with none of the software being particularly superior.

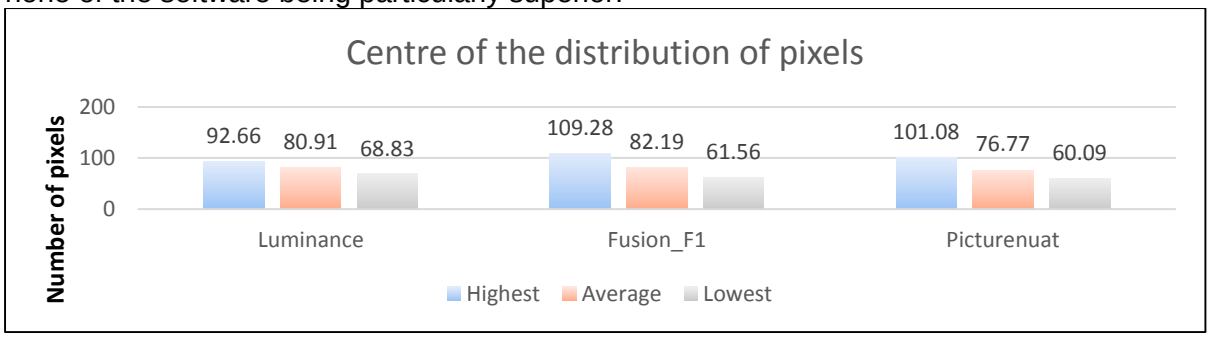

Figure 8. Graph of Centre of the distribution of pixels

7.5.4 Contrast Gradient

The results across the software are also very similar with the only exception of Picturenaut having the smallest 'Highest' gradient magnitude.

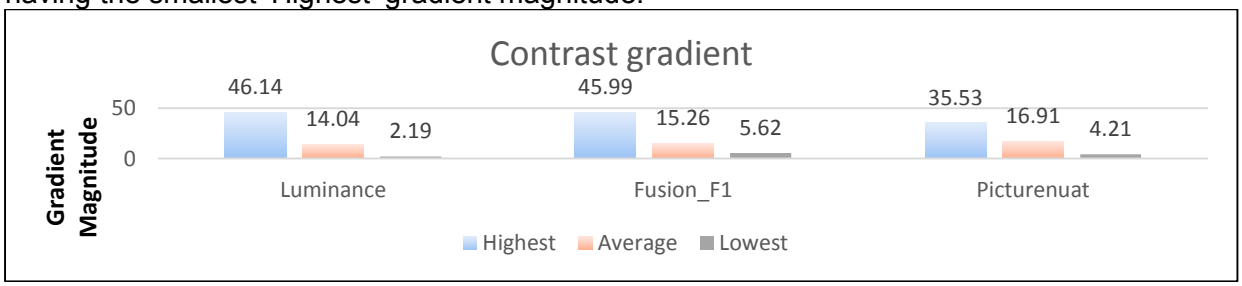

Figure 9. Graph of Contrast gradient

5. Analysis of Findings

With the results of the deviation of pixels and contrast gradient being similar, all three software have similar performance in terms of these two aspects. However, for clipped pixels and unused data from the entire dynamic range, Fusion_F1 and Luminance produced the best results respectively. Fusion_F1 is the most optimal HDRI software because it has the lowest percentage of 1.79% for clipped pixels, a significant decrease from the other two software (Fig. 6). Although Fusion_F1 performed worst at utilising all the data from the entire dynamic range, it is not as significant as the clipped pixels. This is because majority of the data from the HDRI is taken from the centre of the dynamic range, with the other two exposures compensating what the centre exposure is lacking. Thus, Fusion_F1 is the most optimal software for HDRI production.

Lastly, the best EV is determined by finding out how much each aspect differed from the average. The EV (+2, 0, -2) is determined to be the best. Noting that clipped pixel, pixel, unused data and pixel deviation have to be as low as possible while the contrast gradient has to be as high as possible, EV (+2, 0,-2) performs the best compared to others (ANNEX A). A

comparison of EV (+2, 0,-2) against the average is shown here to illustrate the performance of EV (+2, 0,-2).

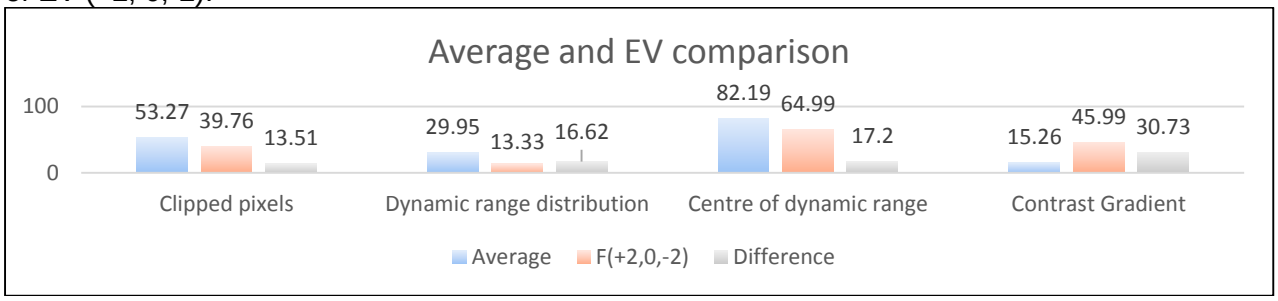

Figure 10. Graph of Average and EV comparison

6. Relevance to Practical Application

9.1 Future Developments

Throughout the research, the experiment has to be done in the absence of rain in order to isolate other significant contributing factor to RFI. During rain, lightning may occur and in turn affect the radio waves (NASA, 2013). However, most of the time, radio interference becomes worse during rain and storms where the clouds intensify more than on clear weather. To serve a more practical purpose, possible further work could be to image dark clouds and compare them with the radio interference data to find out whether the intensity of clouds is also a factor of the interference.

HDRI processing can be applied to highly accurate and precise 3-dimensional reconstruction of the sky and contribute to the research for reducing radio interference. Alternative uses of this research can also be used for other 3-dimensional reconstructions besides the sky. A 3-dimensional reconstruction of a training facility or camp could be used for a realistic simulation training or preparation for possible scenarios to prepare soldiers for combat.

7. Conclusion

With concluding results of Fusion_F1 and the exposure bracket of (+2, 0, -2) at AV22 to be used for the capture of sky images, automation of the production of sky images and HDRI can begin. This would also mean acquiring higher fidelity images to help aid in computer simulation 3-dimensional reconstruction of the sky. Some problems that may occur would be the practicality of research conditions and synchronisation of simultaneous capture of different exposure brackets. However, these can be improved through conducting further experiments in different weather conditions and using three synchronised cameras to capture the exposure brackets simultaneously.

ANNEX A

Legend	Best	Good	Worst

A (+1,0,-1)	Luminance	Fusion_F1	Picturenaut
Clipped Pixels	62.45%	58.86%	61.78%
Distribution within the whole dynamic range	32.16%	21.96%	23.53%
Centre of the distribution of pixels	92.0204	79.5942	81.3236
Contrast gradient in image	2.1881	14.9639	7.2829
B (0,-2,-4)			
Clipped Pixels	65.50%	61.34%	61.38%
Distribution within the whole dynamic range	0.78%	17.25%	54.12%
Centre of the distribution of pixels	81.9822	81.625	101.0826
Contrast gradient in image	5.6711	12.9321	4.2137
C (+4, +2, 0)			
Clipped Pixels	42.82%	47.34%	48.98%
Distribution within the whole dynamic range	30.98%	23.53%	0.39%
Centre of the distribution of pixels	92.2323	61.5648	62.4943
Contrast gradient in image	46.1419	10.8032	35.5321
D(+3,+2,+1,0,-1,-2,-3)			
Clipped Pixels	65.79%	62.39%	31.68%
Distribution within the whole dynamic range	8.63%	12.94%	13.33%
Centre of the distribution of pixels	92.6576	73.7988	55.1816
Contrast gradient in image	4.959	5.6208	27.6205
E (+2,+1,0,-1,-2)			
Clipped Pixels	60.87%	62.57%	65.36%
Distribution within the whole dynamic range	0.78%	32.94%	4.31%
Centre of the distribution of pixels	71.1102	85.3102	81.8806
Contrast gradient in image	10.5985	11.3651	15.7553
F (+2,0,-2)			
Clipped Pixels	53.34%	39.76%	58.99%
Distribution within the whole dynamic range	5.49%	13.33%	0.39%
Centre of the distribution of pixels	68.8342	64.9938	74.4996
Contrast gradient in image	17.0681	45.9913	20.0639
G (+1,-1,-3)			
Clipped Pixels	46.34%	65.35%	43.90%
Distribution within the whole dynamic range	15.69%	36.86%	10.98%
Centre of the distribution of pixels	75.5948	86.7397	60.0901
Contrast gradient in image	23.4973	16.0519	25.9867
H (+2'3,0,-2'3)			
Clipped Pixels	62.11%	61.54%	63.98%
Distribution within the whole dynamic range	10.98%	30.20%	3.53%
Centre of the distribution of pixels	78.6877	87.5806	81.722
Contrast gradient in image	7.6186	13.72	14.0603
I (-2'3,- 1 2'3, -2 2'3)			
Clipped Pixels	54.71%	1.74%	62.38%
Distribution within the whole dynamic range	13.33%	41.57%	7.84%
Centre of the distribution of pixels	73.5712	72.7729	76.1819
Contrast gradient in image	15.2034	18.406	10.6948
J (+1'3,-1 1'3,-2 1'3)			
Clipped Pixels	56.27%	63.07%	65.61%
Distribution within the whole dynamic range	21.57%	40.39%	7.06%
Centre of the distribution of pixels	81.9941	100.8758	86.4357

Contrast gradient in image	14.2535	5.4379	17.4717
K (+1'3,0,-1'3)			
Clipped Pixels	61.78%	62.10%	63.34%
Distribution within the whole dynamic range	23.53%	58.43%	11.76%
Centre of the distribution of pixels	81.3236	109.2794	83.5564
Contrast gradient in image	7.2829	12.5807	7.3642

	Rank 1	Rank 2	Rank 3
Luminance	3	5	3
Fusion_F1	5	1	5
Picturenaut	3	5	3

ANNEX B

```
% Image quality estimation for LDR and HDR images

% Modify the filename of the images here
filename = 'K.jpg';

im = rgb2gray(imread(filename));

% Measure of clipped pixels
h = imhist(im);
clipped = (sum(h(1:10)) + sum(h(end-10:end)))/sum(h);
disp('Proportion of clipped pixels in the image:')
disp('(The lower the better)');
disp([num2str(clipped*100), ' %']);
disp('-----')

% Measure of the distribution within the whole dynamic range
unused = h < sum(h(11:end-11))/1000;
disp('Proportion of "unused" parts of the dynamic range')
disp('(The lower the better)')
disp([num2str(sum(unused)/2.55), ' %'])
disp('-----')

% Measure of the center of the distribution of the pixels
center = mean(im(:)) - 127;
disp('Deviation from the center of the dynamic range');
disp('(The smaller the better)')
disp(num2str(abs(center)))
disp('-----')

% Measure of the amount of gradient in the image
grad = imgradient(im);
disp('Amount of contrast in the image (gradient)');
disp('(The larger the better)')
disp(num2str(sum(double(grad(:))/(size(im,1)*size(im,2)))));
```

References

Army Study Guide. (1999). *Communication.* Retrieved from Army Study Guide: http://www.armystudyguide.com/content/army_board_study_guide_topics/communications/communications-study-guid.shtml

Attali, D., & Lachaud, J. O. (2001). Computational Geometry. *Delaunuay conforming iso-surface, Skeletion extraction and noise removal*, 175-189.

Camalan, M. (2006, September). The importance of Ionosphere in Radio Communication. *The Fountain Magazine*.

Cambridge in colour. (2005, May 24). *Understanding lens flare.* Retrieved from Cambridge in colour: http://www.cambridgeincolour.com/tutorials/lens-flare.htm

Ford, S. (2000, April). *An Amateur Satellite Primer.* Retrieved from ARRL, the national association for Amatuer Radio: http://www.arrl.org/files/file/Technology/tis/info/pdf/0004036.pdf

Hallas, J. R. (2009, May 14). *A quick look at radio frequency interference.* Retrieved from ARRL, the national association for Amateur Radio: http://www.arrl.org/files/file/Technology/RFI%20Main%20Page/Hallas.pdf

Kenyon, H. (2012, March 15). *More satellites means more SATCOM gridlock.* Retrieved from GCN: http://gcn.com/articles/2012/03/14/satellite-2012-satellites-antennas-interference-rates.aspx

NASA. (2013, June 27). *Samples of Radio Interference.* Retrieved from Radio Jove NASA: http://radiojove.gsfc.nasa.gov/observing/rfi_samples.htm

Phatz, T., Herrmann, H. J., & Shinbrot, T. (2010, April 11). Why do particle clouds generate electric charges? *Nature Physics 6.5*, 364-368. Retrieved from Nature Publishin Group: http://www.nature.com/nphys/journal/v6/n5/full/nphys1631.html#a1

Poole, I. (1999, November). *Radio Waves and the Ionosphere.* Retrieved from ARRL, the national association for Amateur Radio: http://www.arrl.org/files/file/Technology/pdf/119962.pdf

Radio Jove Nasa. (2006, September 28). *The Effects of Earth's Upper Atmosphere on Radio Signals.* Retrieved from Radio Jove: http://radiojove.gsfc.nasa.gov/education/educ/radio/tran-rec/exerc/iono.htm

Rouse, M. (2010, March). *Electromagnetic interference.* Retrieved from SearchMobileComputing: http://searchmobilecomputing.techtarget.com/definition/electromagnetic-interference

Stumpfel, J., Jones, A., Wenger, A., Tchou, C., Hawkins, T., & Debevec, P. (2004). Direct HDR Capture of the Sun and Sky. *In Proceedings of the 3rd international conference on Computer Graphics, Virtual Reality, visualisation and interaction in Africa*, 145-149.

Willert, C., & Gharib, M. (1992). Experiments in Fluids. *Three-dimensional particle imaging with a single camera*, 353-358.